THE ASTROPHYSICAL JOURNAL, 411:594–601, 1993 July 10

IONIZED ABSORBERS, IONIZED EMITTERS, AND THE X-RAY SPECTRUM OF ACTIVE GALACTIC NUCLEI

HAGAI NETZER
Laboratory for High Energy Astrophysics, Code 666, NASA/Goddard Space Flight Center, Greenbelt, MD 20771;[1]
e-mail: B:netzer@wise.tau.ac.il
Received 1992 July 2; accepted 1993 January 11

ABSTRACT

Broad absorption features are common in the X-ray spectrum of low-luminosity AGNs. The features have been modeled by leaky neutral absorbers or by highly ionized gas that completely occult the continuum source. Such models are incomplete since they do not take into account all the physical processes in the gas. In particular, no previous model included the X-ray emission by the ionized absorbing gas and the reflection of the continuum source radiation. The present work discusses the emission, absorption, and reflection properties of photoionized gases with emphasis on conditions thought to prevail in AGNs. It shows that such gas is likely to produce intense X-ray line and continuum radiation and to reflect a sizable fraction of the nonstellar continuum at all energies. If such gas is indeed responsible for the observed X-ray absorption, then absorption edges are much weaker than commonly assumed, and some residual X-ray continuum is likely to be observed even if the line of sight is completely blocked. Moreover, X-ray emission features may show up in sources not showing X-ray absorption. This has immense consequences for medium-resolution X-ray missions, such as *BBXRT* and Astro-D, and for the planned high-resolution experiments on board *XMM* and *AXAF*.

Subject headings: galaxies: active — X-rays: galaxies — X-rays: general

1. INTRODUCTION

Many low-luminosity Seyfert galaxies, and other active galactic nuclei (AGNs) show clear evidence of X-ray absorption at energies around 1 keV (e.g., Reichert et al. 1985; Turner et al. 1991 and references therein). This has been interpreted as due to material on the line of sight which can be either "cold" (neutral or of very low ionization) or "warm" (highly ionized). Hereafter we refer to the above two cases as the "neutral" or the "ionized" absorber.

The neutral absorber spectrum is recognized by the large optical depth at energies above 1 Ry and the recovery to the original, incident continuum level at $\sim$1–4 keV. The exact shape and energy of that recovery depends on the column density of the absorber, most importantly the oxygen column along the line of sight. Such a pure absorption spectrum is hardly ever observed and a more typical AGN spectrum shows a gradual increase in absorption in the range 0.3–0.9 keV, to a few percent of the continuum level and decreasing absorption at higher energies. In absorbed spectra, the radiation observed at $\sim$0.5 keV, where absorption by neutral gas should be complete, has been interpreted as either due to a highly ionized absorber, or alternatively, a leaky neutral absorber (the so called "partial covering" case). In the leaky absorber case, the covering fraction along the line of sight is less than unity and part of the central continuum is observed through the clouds. This has been discussed extensively by Holt et al. (1980), Reichert et al. (1985), Reichert, Mushotzky, & Holt (1986), Wachter, Strauss, & Filippenko (1988) and others. The ionized absorber case has been discussed from a physical viewpoint by Krolik & Kallman (1984) and in relation to AGN spectra by Halpern (1984), Yaqoob, Warwick, & Pounds (1989), Pan, Stewart, & Pounds (1990), Yaqoob & Warwick (1991) and others. A related, although different idea of very high density material in AGN centers, with consequences to the observed X-ray spectra, has been discussed by Ferland & Rees (1988).

While some partial covering or ionized absorber models give reasonable fits to observed AGN X-ray spectra such models leave much to be desired. In particular, important processes in the absorbing gas, such as X-ray line and continuum emission and reflection by free electrons, have not been considered. The only exception is some work on collisionally ionized gas, thought to be the intercloud medium in the broad-line region (BLR; see Kaastra, Mewe, & Brinkman 1989). There are difficulties with the idea of hot intercloud gas (e.g., Mathews & Ferland 1987), and it will not be discussed here any further. The present work discusses high-energy processes in photoionized gas near the center of AGNs and demonstrates the basic X-ray spectral properties. This is important to X-ray observations since some of the newly discussed features are within the resolution capability of medium (*BBXRT*, Astro-D) missions and will be easily detectable by the high-resolution instruments on board *XMM* and *AXAF*. Section 2 describes the new calculations and demonstrates the absorption, emission and reflection spectrum of ionized absorbers. Consequences to the X-ray spectrum of AGNs are discussed in § 3 and summarized in § 4.

2. EMISSION, REFLECTION, AND ABSORPTION BY IONIZED ABSORBERS

We are interested in the emission, reflection and absorption properties of material near a central source of ultraviolet and X-ray radiation. We assume this to be the only source of heating and excitation for the gas and do not consider shocks, mechanical heating, and nonequilibrium situations. The central continuum radiation is approximately known, and the problem is well defined once the properties of the surrounding gas are specified.

We assume for simplicity that the nuclear gas is made up of a spherical distribution of clouds, with typical dimensions much

[1] On sabbatical leave from the School of Physics and Astronomy, the Raymond and Beverly Sacler Faculty of Exact Sciences, Tel Aviv University.

smaller than the distance to the center (a thin shell geometry is used for most applications). The clouds can be smaller or larger than the central X-ray source. We further assume that all clouds have about the same density and column density in the radial direction, but not necessarily the same lateral dimension. We consider in detail only a small range of densities, around 10^{10} cm^{-3}, but the entire range of 10^{9}–10^{12} cm^{-3} was investigated and most results discussed below are quite general. A likely, although not the only location for such material is just inside the BLR, since its density is similar to BLR densities and the assumed ionization parameter (see below) is similar or higher. Another possibility is lower density gas outside the BLR. As shown below, such gas will escape the detection of most optical and ultraviolet observations. We do not consider the very high density, optically thin material discussed by Ferland & Rees (1988).

The covering fraction of the cloud system is f_c, and we distinguish between two cases regarding the obscuration of the central source. The first is a situation where the clouds are small compared with the continuum source size. The fraction of the continuum obscured by the clouds, along any line of sight, is f_c. This is the partial covering case mentioned earlier and discussed in numerous X-ray related papers. We note that the case of a single large cloud obscuring a fraction f_c of the source is identical to this situation for all practical purposes. In the second case, some clouds may be larger than the X-ray continuum source which results in fractional obscuration, along some line of sights, larger than f_c. We consider this case in the limit of complete obscuration and refer to it as the *Large Cloud Case.*

The emission and absorption spectrum of the clouds can be calculated in a straightforward way by solving the ionization and thermal structure at every point in the gas. This produces a depth-dependent opacity, for each frequency, and the necessary emission coefficients for the different lines and continua. The method is quite standard, although rather complicated, since a large number of atomic processes must be treated. In particular, high-density, large optical depth clouds may be present and interactive procedures must be applied to correctly solve for the optical depth. Many details of such calculations, and relevant references, are given in Rees, Netzer, & Ferland (1989) and a more general description can be found in Netzer (1990). X-ray opacity is obviously of major importance. Discussion of it can be found in Krolik & Kallman (1984) and Ferland & Rees (1988). The numerical code used in this work is ION, most recently described in Rees et al. (1989). A typical (single cloud) model with this code includes the solution for the ionization structure and temperature in 100–200 zones, and a definition of the radiation field at $\sim$260 frequency points. The present version was extended to include a more complete treatment of X-ray related processes, such as the Auger ejection of up to three inner electrons, the depth dependent transfer of most recombination continua and X-ray emission lines. Relevant details are given below.

The continuum used for the present calculations is listed in Table 1. It is made of an infrared source peaking (in νF_ν) at 9 μm, an optical-ultraviolet "blue bump," made of a broken power law with an optical energy spectral index of $\alpha = 0.5$ ($F_\nu \propto \nu^{-\alpha}$), and an X-ray power law continuum with spectral index of 0.7 extending up to 40 keV. The ultraviolet–to–X-ray index, α_{ox}, is 1.2, typical of Seyfert 1 galaxies and radio-loud quasars. This continuum is similar to the one discussed by Mathews and Ferland (1987), Rees, Netzer, & Ferland (1989) and several other recent papers. It is also similar to a combination of a thin accretion disk spectrum and a power law X-ray source, known to give a good fit to the spectrum of many AGNs (e.g., Laor 1990). The gas composition is approximately solar and is given by

TABLE 1

ASSUMED CONTINUUM

Energy (Ry)	log F_ν (normalized)
1.5×10^{-6}	12.0
1.0×10^{-3}	15.02
1.0×10^{-2}	14.52
0.12	13.37
3.0	12.67
20.0	10.61
3.5×10^{3}	9.036
1.0×10^{6}	1.0

$$(\mathrm{He, C, N, O, Ne, Mg, Si, S, Fe}):\mathrm{H} = (1000, 3.7, 1.1, 8.0, 1.0, 0.35, 0.33, 0.16, 0.4) \times 10^{-4}$$

The dimensionless ionization parameter, U, is defined as the ratio of the incident ionizing photon flux over $N_{\mathrm{H}}c$, where N_{H} is the hydrogen number density and c the speed of light. For the above chosen continuum, the fractional ionization of hydrogen is $\sim N_{\mathrm{H}^+}/N_{\mathrm{H}^0} \simeq 10^6 U$, and the column density of ionized gas, in an infinitely thick medium, is $\sim 10^{23.3} U$ cm^{-2}. The results shown include all column densities up to $10^{23.5}$ cm^{-2} and cover the range $0.3 \leq U \leq 10$. (There is no fundamental reason to limit the discussion to this range, only practical considerations to do with the coherent presentation of results.) For comparison, the ionization parameter that best fits the observed broad line spectrum of AGNs, with this continuum, is $\sim$0.3 and the typical column density is thought to be 10^{23} cm^{-2}.

2.1. *Absorption Spectrum*

Figure 1 shows the calculated absorption spectrum of a gas cloud with a constant hydrogen density of 10^{10} cm^{-3}, column density of 10^{23} cm^{-2} and three ionization parameters, $U = 1$, 3, and 10. Clearly visible are the strong absorption edges (marked) of the most abundant ions, such as O^{+6}, O^{+7}, and C^{+5}. Note that the $U = 1$, lowest ionization model, approaches the neutral absorber case. The absorption properties are almost identical for this and other low-ionization material of similar column density. Hereafter we refer to all cases of $U \leq 1$ as "low-ionization" cases. The exact shape of the observed continuum between 1 and 4 keV depends, however, on the gas composition in particular the oxygen abundance.[2]

As for the absorption properties of the warm absorbers ($U = 3$,10), these are characterized by a minimum around 1 keV, due mainly to oxygen, and weaker, broad absorption features due to carbon and nitrogen. The strength of all features decreases with increasing U up to a case of no absorption, corresponding to a fully ionized gas. The overall shape explains the appeal of such models in explaining X-ray spectra with maximum absorption around 1 keV. Note in particular the stratification implied by the strong absorption edges. Such

[2] Note in Fig. 1 that a factor of 3 in U makes five orders of magnitude difference in opacity at $E \sim 800$ eV.

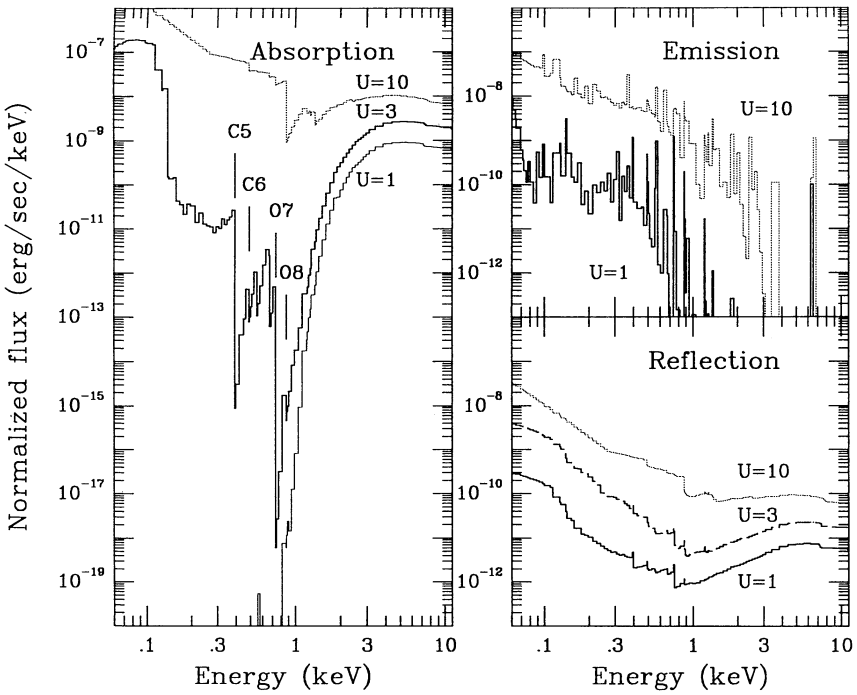

FIG. 1.—The absorption, emission, and reflection spectra of photoionized gas with hydrogen density of 10^{10} cm^{-3} and column density of 10^{23} cm^{-2}, exposed to the ionizing continuum of Table 1, with ionization parameter (U) as marked. The absorption spectrum for lower ionization parameters is very similar to the $U = 1$ case shown and is typical of "neutral absorbers." Note the nonuniform resolution used for displaying the data (peak intensities should not be confused with total intensity).

clouds have metal ionization fronts, at different locations, and there is no way to accurately calculate their absorption properties without complete modeling and a full depth-dependent solution of the ionization and thermal structure. The strength of several absorption edges depends, to a large extent, on the unobserved ultraviolet continuum radiation which produces most of the ionizing radiation.

Previous attempts to calculate an ionized absorber spectrum were either incomplete or else gave very little information about the physics that go into the model. The recent paper by Pan et al. (1990) makes use of a sophisticated photoionization code (CLOUDY, by G. Ferland) which is similar to the one used here. However, these authors approximated the ultraviolet continuum by extrapolating the observed X-ray spectrum to lower energies, retaining the same slope. This is a poor approximation to the ultraviolet spectrum of AGNs, which results in considerable differences in the ionization structure. Yaqoob et al. (1989) treated the case of NGC 4151 and used a "modified version" of CLOUDY which is not described, or illustrated in their paper. Yaqoob & Warwick (1991) used a simplified model which, given the results presented here, is less than adequate. None of the above-mentioned papers considered emission or reflection by the ionized gas, as described below.

2.2. *Emission Spectrum*

Several mechanisms give rise to X-ray emission features in photoionized gases. X-ray lines are the result of collisional excitation, inner shell fluorescence and recombination. X-ray continua are due to recombination and two-photon decay. There is very little discussion of such features in photoionized gases, with the exception of Ferland & Rees (1988), who considered only the very high density, optically thin case and did not include line emission. On the other hand the X-ray spectrum of collisionally excited gases is well covered (e.g., Raymond & Smith 1977; Mewe 1991 and references therein), although the range of densities usually considered is small and optical depth effects are not included. Needless to say, none of the available hot-plasma calculations can be applied to the situation discussed here.

The present work treats all important emission processes in a photoionized gas. Bound free continua are calculated with the full frequency and optical depth dependence, taking into account ground-state recombination of all species and level 2 recombination of hydrogen-like ions. Most absorption cross sections used in this work are from Reilman & Manson (1979) and the corresponding recombination rates are from Shull & Van Steenberg (1982) and Pequignot, Petitjean & Boisson (1991). The notable exception are iron ions for which improved recombination rates are available (Arnaud & Raymond 1992). The fraction of all recombination leading to the ground is either taken from existing references (e.g., Gould 1978; Pequignot et al. 1991) or else estimated from the absorption cross section. A simple energy dependence for the recombination continuum, derived from an assumed $a_\nu \propto \nu^{-s}$ energy dependence of the absorption cross section (not the actual Reilman & Manson's data), is used. Here $s = 2.8$ is assumed for H-like ions and $s = 2$ for all others. There is no need for more accurate treatment of the recombination continua since the temperature of the photoionized gas is typically well below the equilibrium temperature of the ion in question. Thus, such a continuum forms a narrow emission feature near the ionization edge, and its shape is largely controlled by the exp $[(I - h\nu)/kT_e]$ term. For example, the typical half-width of the oxygen recombination continua above 739 (O VII) and 871 (O VIII) eV is only $\sim 10\,(T_e/10^5\ \mathrm{K})$ eV, where the electron temperature is an increasing function of U and $T_e \simeq 1.3 \times 10^5$ K

for $U = 3$. For H-like ions, the complete $2s$, $2p$ equilibrium population, taking into account the scattering of the Lα line photons and all other processes, is solved at each location. The resulting $2s$ level population is then used to calculate the two-photon continuum. A critical number is the $2s$–$2p$ collision cross section which, for the densities under discussion, is an important depopulation mechanism for the $2s$ level. The hydrogenic value for protons and electrons, scaled by the charge of the ion, was assumed for this rate. He-like ions are also treated in detail, solving, at each point, the statistical equilibrium equations for the 2^1S, 2^1P, 2^3S and 2^3P levels, and including optical depth in all transitions. Finally, free-free emission is also added to the emitted flux.

The transfer of the locally produced continuum radiation is done in a way appropriate for a slab geometry, assuming isotropic emission. We illustrate this below to discuss the dependence on the covering factor. Assume a point in the cloud and a frequency ν such that the local emission coefficient is j_ν, the optical depth to the inner (illuminated) surface is τ_ν and the total optical depth is T_ν. Part of this radiation escapes and contributes an amount of dF_ν to the emergent flux. The rest is subsequently absorbed on the way out. The absorbed part is added to the local radiation field in the outward direction and is allowed to interact with that material. Here we generalize the treatment of dF_ν to include absorption by other clouds, with the given covering factor f_c and the assumption of a thin shell geometry, thus

$$dF_\nu = 2\pi j_\nu f_c[E_2(T_\nu - \tau_\nu) + (1 - f_c)E_2(\tau_\nu) + f_c\, E_2(T_\nu + \tau_\nu)] \simeq 2\pi j_\nu f_c[\exp(-\tau_{\rm out}) + (1 - f_c)\,(\exp -\tau_{\rm in}) + f_c\, \exp(-2\tau_{\rm in} - \tau_{\rm out})]\,, \quad (1)$$

where $E_2(\tau)$ is the second exponential integral. The second expression on the right assumes that the transfer to the inner and outer surfaces can be approximated by mean, frequency-dependent inward ($\tau_{\rm in}$) and outward ($\tau_{\rm out}$) optical depths. This is not used in the calculations and is given only to illustrate the three important limits to this expression.

1. Optically thin material ($\tau_{\rm in} \ll 1$, $\tau_{\rm out} \ll 1$). The observed flux is simply proportional to $f_c j_\nu$, i.e., to the amount of emitting gas.

2. The inward and outward optical depths are about equal ($\tau_{\rm in} \simeq \tau_{\rm out} = \tau$). This may happen when the total optical depth is of order unity. The contribution to the observed emission is $\sim 2\pi j_\nu \exp(-\tau)(2f_c - f_c^2)$ and is an increasing function of the covering factor.

3. The gas is optically thick and $\tau_{\rm in} \ll \tau_{\rm out}$. The first and the third terms in equation (1) can be omitted and the observed flux is proportional to $2\pi j_\nu \exp(-\tau_{\rm in})(f_c - f_c^2)$ which peaks at $f_c = 0.5$. (To put it differently, for very large covering factors, the loss due to absorption by other clouds is more important than the extra emission due to the increase in f_c.) Case 3 is the one most relevant to the situation assumed here of centrally illuminated large column density clouds.

The most intense X-ray emission lines are also included in the calculations. These are the Lα, Hα, and Hβ lines of H-like ions, $1\,^1S$–2^1P, $1\,^1S$–2^3S and $1\,^1S$–2^3P transitions in He-like ions, iron Kα lines and the strongest collisionally excited lines of all elements. Some of the lines can provide important diagnostics of the physical conditions in the gas. For example lines of He-like ions are good density calibrators. For the sake of simplicity and because the planned high-resolution X-ray missions will take years to fly, it was decided to omit any detailed discussion of this kind.

Optically thick lines are treated with the escape probability method taking into account the destruction of line photons by continuous opacity (e.g., Netzer 1990), which is very important for all models presented here. The absorption of line photons by clouds on the other side of the source is calculated in a way similar to equation (1), assuming that the relative velocity of clouds is much larger than the local Doppler width. Several recombination L-shell lines of iron ions are expected in the energy range 800–1200 eV (e.g., Band et al. 1990; Liedahl et al. 1990). Such lines are in fact observed in the *BBXRT* spectrum of NGC 1068 (Marshall et al. 1993) and are suspected in other sources (Turner et al. 1991). The poorly known atomic data limits the treatment of such transitions. Here we simply assumed that 40% of all the recombinations of Fe17–Fe24 produce such lines and the radiation is equally divided between the two strongest resonance lines of the ion in question. The production of iron Kα fluorescence lines, in neutral gas, has been considered in great detail (e.g., George & Fabian 1991) but little has been done to estimate their strength in ionized gases. All examples shown in this paper have small enough Compton depth to neglect the effect of scattering on the lines. In this case the calculation of the Kα line intensity is straightforward and need no further discussion.

The emission spectrum of the 10^{23} cm^{-2} column density clouds discussed earlier, with the same range of ionization parameters, is shown in the right-hand panel of Figure 1. Only two values of U are shown, to avoid a confusion due to the large number of features. Note the strong, sharp line and edges, of carbon, oxygen, neon, and iron and the broadening of the recombination continua, due to the increase in temperature, in the larger U case. Obviously, the emission is strongest at the energy where the absorption is most noticeable, which has important consequences to the observed spectrum.[3]

2.3. *Reflection Spectrum*

Compton reflection and its affect on the X-ray spectrum has been discussed in several papers (e.g., Bai & Ramaty 1978), especially since the work of Lightman & White (1988). The main emphasis has been on reflection by neutral accretion disk material (e.g., Matt, Perola, & Piro 1991; George & Fabian 1991) and little attention was given to ionized gas. Done et al. (1992), described the reflection by ionized material in Cygnus X-1. These authors used the Lightman & White (1988) expression for a uniform, constant opacity medium, and applied it to their own ionization calculation which assumed constant temperature and no depth dependent opacity. Such calculations are only rough approximations to the more realistic case, where the ionization and temperature, and therefore the gas opacity, change with depth. There is little discussion, if any, of the reflection properties of gas with small Compton depth.

The present calculations include reflection by bound and free electrons by evaluating, at each point and frequency, the fraction of the incident continuum flux that is scattered and escape from the cloud. This is obtained from the local ratio of the Compton and total opacity, and the optical depth, under the assumption that half of the reflection is in the inward direction. The radiation is transferred to the inner surface in a way

[3] The resolution used to display the data is not uniform, and one should not confuse the peak intensity of the lines with their intensity.

similar to that of the diffuse continuum (eq. [1]) with the correct dependence on f_c. This treatment was checked against the Lightman & White's (1988) two-stream approximation in the two limits of scattering and absorption dominated atmospheres. The overall agreement is better than 10%. It was also verified that a complete depth-dependent solution gives, in most cases, results that are substantially different from a simple application of the Lightman & White's (1988) expression.

The amount of reflection by highly ionized gas is never very small. For an absorption dominated atmosphere it can be approximated by the smaller of $\sigma_e/4\sigma_{ab}$ and $0.5[1-\exp(-\tau_e)]$, where τ_e is the total Compton depth. Minimum reflection is at the frequency where σ_e/σ_{ab} is minimal which, for most examples given here, is just beyond the O8 absorption edge at 871 eV. A better estimate must include a dependence on the ionization parameter that determines the gas opacity. For example, an estimate of the reflection just beyond 871 eV can be obtained by noting that for $U \sim 5$ all oxygen is O^{+7} or O^{+8} and $O^{+8}/O^{+7} \sim 0.4U$. Given the ionization cross section for oxygen, the reflected continuum flux for this range of U is

$$F_{\rm ref} \simeq 2 \times 10^{-6} \frac{0.4U+1}{N_{\rm O}/N_{\rm H}} f_c(1-f_c)F_{\rm cont}\,, \qquad (2)$$

where $F_{\rm cont}$ is the incident flux. Thus, for a solar composition material, the minimal amount of reflection is of the order of $0.01f_c(1-f_c)$. The fraction can be considerably larger at lower and higher energies. Figure 1 shows the calculated reflected spectrum for the clouds considered earlier.

2.4. *Observed Spectrum*

The observed X-ray spectrum is the sum of the emission, absorption, and reflection components. These are combined here in two different ways, corresponding to the partial covering and the large cloud scenarios. Figure 2 shows this for $U = 3, f_c = 0.5$ and the cloud discussed earlier. The left-hand side of the diagram shows the three components separately and the right-hand side the two ways they were combined. The large cloud case is dominated by absorption while the partial covering case shows only weak spectral features and almost a constant depression, by a factor of $1-f_c$, relative to the incident continuum. Most realistic cases should fall somewhere between those two. Typical to this and other cases is the big difference between pure absorption (the only case considered in previous works) and the realistic spectrum, where emission and reflection are included (compare the pure absorption, solid line on the left-hand side of Figure 2 with the lower curve on the right). Most absorption edges are weaker, line and linelike features are prominent, especially inside the absorption through, and reflection provides a firm lower limit to the depression of the observed spectrum relative to the continuum. The lower right panel of the diagram shows the same calculated spectra plotted with typical medium X-ray resolution such as in *BBXRT* and Astro-D. All this has important consequences to the study of AGNs, as discussed in the following section.

3. APPLICATIONS TO AGNs

3.1. *Partial Covering and Absorption Edges*

The X-ray spectrum of many low-luminosity AGNs shows a clear decline and subsequent recovery, over the energy range 0.5–4 keV. This has been modeled as partial covering by a neutral absorber or complete covering by an ionized absorber. The lowest absorption point is typically one to two orders of magnitude below the extrapolated continuum, implying a

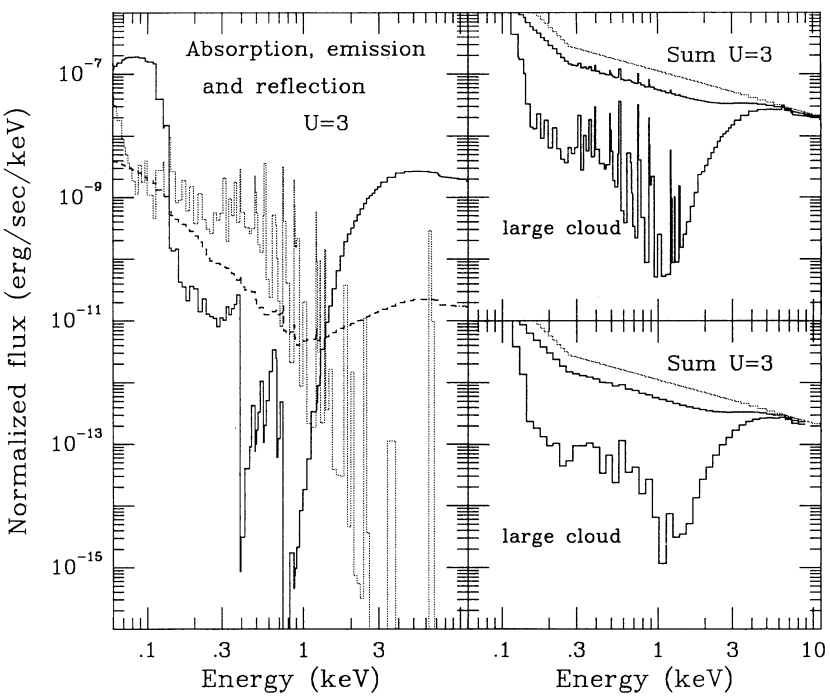

FIG. 2.—Left: The three X-ray spectral components, absorption (*solid line*), emission, (*dotted line*) and reflection (*dashed line*), of the $U = 3$ cloud of Fig. 1. *Top right*: Two possible combinations of the observed spectrum. A single large cloud that completely obscures the continuum source (*lower curve*) and a system of many clouds much smaller than the continuum source (*middle curve*). The covering factor in both cases is 0.5. The incident continuum (*upper dotted line*) is shown for comparison. *Bottom right*: The same but as would have been observed by a medium-resolution X-ray experiment with $E/\Delta E \simeq 10$.

covering factor of 90%–99%. In some objects (e.g., NGC 4151; see Yaqoob et al. 1989), the covering fraction by a cold absorber was claimed to change in time which was interpreted as cloud motion across the continuum source.

The calculations presented here suggest an alternative to the partial covering scenario, involving full obscuration of the continuum but very different from previous ionized absorbers models. In this case, clouds on other sides of the continuum source reflect a fraction of the incident continuum into our line of sight. For low ionization parameters, the minimal amount of reflected flux is of the order of few times $10^{-3}F_{\rm cont}$. For large ionization parameters it can be larger (Fig. 1 and eq. [2]). Thus, complete covering of the central source by low-ionization material cannot be ruled out by observations showing residual X-ray flux.

X-ray absorption edges are used, extensively, to deduce the column density of different ions. The present work demonstrates how such edges are modified, in shape and in depth, to the extent that they may escape detection. Figure 3 shows several more examples of ionized absorbers, this time for somewhat different density, column density, and covering factors. In the $U = 3$ large column density cloud shown on the right, the emission and reflection almost completely mask the appearance of the strong O8 edge. This edge is clearly visible in the smaller column cloud, where emission is not so strong. Note also that emission is quite prominent even for a covering as small as 0.1.

3.2. *Line and Linelike Features*

The width of the X-ray emission lines is of course unknown. A reasonable guess will make it comparable to the width of the broad optical emission lines, produced by the relative motion of the clouds. Diffuse continuum emission features, that are broad in many astrophysical situations, can be very sharp too, because of the low temperature of the photoionized gas. Their intrinsic (single cloud) width can be small, and their total (many cloud) width may not exceed by much the emission-line width. Such features can easily be confused for emission lines. The intensity of such linelike features is not large. It depends on the column density and the covering factor of the gas, and the depth of the corresponding absorption edges. A crude estimate can be obtained by considering the amount of continuum radiation available at each energy. For example, in highly ionized gas most of the absorption in the 330 eV band between 870 eV and 1200 eV is due to H-like oxygen. About one-third of this absorption results in Lyman continuum emission. Thus, the equivalent width of this emission, measured against the incident continuum, cannot exceed about $110f_c(1-f_c)$ eV. With a typical width of ~ 10 eV, and a reasonably large covering factor, such a feature should be detectable by future high-resolution experiments and perhaps also by Astro-D. However, this linelike feature is likely to be observed against a much fainter, absorbed continuum (Fig. 2), with a considerably larger equivalent width.

X-ray line intensities depend on the column density, covering factor and level of ionization. The following is a short summary of the strongest lines with equivalent width neasured against the unobscured continuum, assuming full coverage, and with a column density of 10^{23} cm^{-2}. For $U < 3$, all lines, except for the iron Kα lines, are weak with equivalent widths not exceeding ~ 10 eV. For $3 < U < 10$, the strongest emission lines are due to He-like ions (Figs. 1 and 3) and iron Kα lines. The oxygen He-like line can exceed, in this case an equivalent width of ~ 20 eV. For $U \sim 10$ and larger, the spectrum is dominated by iron L-shell lines and Lα lines of H-like species. Such Lα metal lines are somewhat stronger than the corresponding Lyman continua, with typical equivalent width of 10–30 eV.

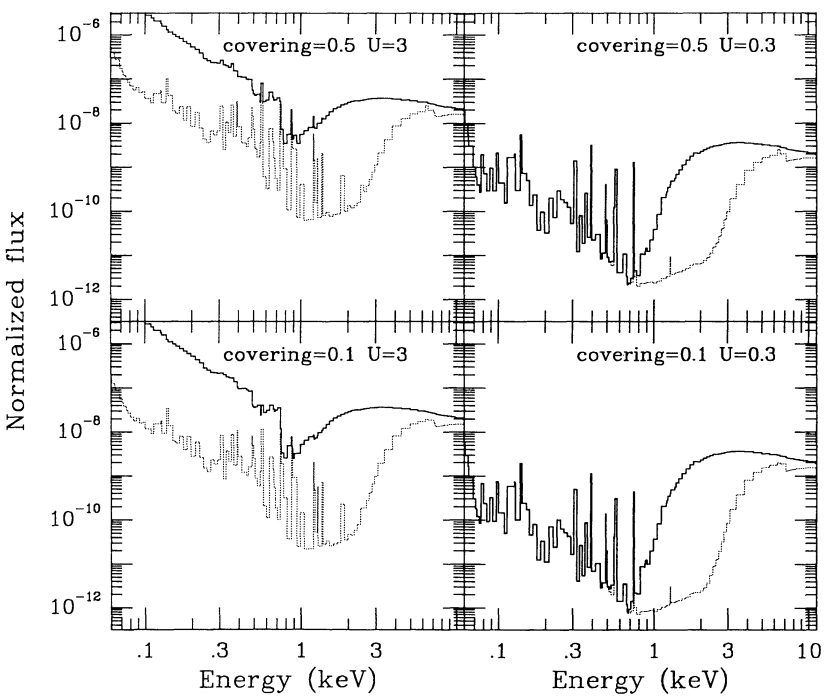

FIG. 3.—Calculated X-ray spectra for the large cloud case. *Left*: $U = 3$, $N = 10^{11}$ cm^{-3} and two covering factors, 0.1 and 0.5. Each box shows two column densities: $10^{22.5}$ cm^{-2} (*solid line, upper curve*) and $10^{23.5}$ cm^{-2} (*dotted line, lower curve*). *Right*: Same for $U = 0.3$; a typical BLR ionization parameter.

Emission-line intensities depend crucially on dielectronic recombination, a process that dominates over radiative recombination at high temperatures. The cascade from high quantum number levels, following such a recombination event, results in a multitude of lines that are most noticeable near the ionization limit. ION includes such lines only for He-like ions. Similarly, three body recombination at high densities enhance the emission lines near threshold energy. Only the H-like and He-like ions shown here include this contribution.

Strong linelike features are possibly seen in *Einstein* SSS spectra of several Seyfert galaxies (Turner et al. 1991). Their measurement is difficult, due to the poor spectral resolution, and their typical equivalent width is 30–100 eV. Some of the features are questionable, due to uncertainties in the fitting procedure, others are probably real. Turner et al. (1991) suggested that the features may be due to hot (0.5–1 keV), collisionally ionized plasma. The present work indicates that photoionized gas may be responsible. This is either the gas seen in absorption, in some cases, or highly ionized gas near the center but with small covering factor. Such material is only detectable through emission and reflection. The energy of the feature is typically $\sim$900 eV and the most likely contributors are the Ne VII and Ne VIII Lα lines, the O VII and O VIII continua and iron L-shell lines.

3.3. *Variability*

Most low-luminosity AGNs are large-amplitude, short timescale X-ray variables. Such continuum flux variations change the ionization and opacity of any nearby gas. For the absorbed sources, instantaneous (hours) adjustment of the absorption spectrum are expected, provided the density is larger than few times 10^8 cm^{-3}, since this material is on our line of sight to the center. This is not the case for emission and reflection produced by material on other sides of the central source. The changes in emission and reflection follow the continuum changes with a lag corresponding to the light crossing time of the system. While the location of the gas is not known, it is likely to be far enough such that the light crossing time is longer than the typical variability time. The interpretation of variable X-ray spectral features is thus more complicated than previously assumed. For example, the spectrum of an X-ray source observed to be on the rise can be a combination of absorption by high-ionization material with emission and reflection from lower ionization (corresponding to earlier times) gas.

3.4. *X-Ray from the BLR and Ultraviolet Emission Lines*

Recent models of the BLR assume the gas in this region to have densities and column densities similar to the ones discussed and demonstrated earlier, with a somewhat smaller ionization parameter (we do not consider different ideas about the origin of the optical lines, such as emission from an accretion disk). The X-ray spectrum of such gas is shown in Figure 3 for the case of hydrogen density of 10^{11} cm^{-3} and two column densities: $10^{22.5}$ cm^{-2} and $10^{23.5}$ cm^{-2}. (The somewhat higher density chosen in this case is mainly for illustrative purposes and the X-ray spectrum of lower density BLR clouds is almost indistinguishable from the one shown.) As evident from the diagram, the overall appearance is similar to the one in the higher U cases. In the BLR cloud case, all the flux between 0.1 and 0.9 keV is due to emission and reflection since none of the central radiation can penetrate the gas. This explains the absence of absorption edges. The main difference in the emission properties is the relative weakness of the broad 0.5 keV feature, due to the low level of ionization (compare the left and right sides of Fig. 3). As mentioned earlier, this work does not consider emission or reflection by a hot intercloud gas.

If gas clouds with the properties suggested earlier are indeed present in AGNs they might produce optical and ultraviolet spectral features that are strong enough to be detected. This was investigated using the models described above. For $U \leq 3$, the only ultraviolet lines of considerable strength are O VI λ1035 and Ne VIII λ774. The O VI λ1035 line is commonly observed in spectra of quasars and it is conceivable that some of it is produced by very high ionization gas. An obvious test is to compare its profile with that of other ultraviolet lines since the high-ionization gas is likely to have different location and velocity. The maximum contribution to the observed line is probably large since for such ionization parameters the line emissivity is well below the one expected in typical broad-line clouds. For $U > 3$ the strongest lines are due to Fe 16–20, at around 100–300 Å. Ne VIII λ774 is the strongest line accessible to the *HST*, with a moderate strength. For the typical conditions considered here, the emissivity of these lines is too small to make them visible even for the largest covering factor. Thus high-ionization material, if present, will be hard to detect at optical and ultraviolet wavelengths.

4. CONCLUSIONS

The presence of an X-ray absorbing gas in low-luminosity AGNs is well established. Such gas is likely to reflect a sizable fraction of the central source radiation and will emit line and continuum radiation at typical energies of 0.1–2 keV. Fitting observed X-ray spectra must include all such processes, not just absorption as in previous works. As demonstrated here, the inclusion of X-ray reflection and emission can considerably change the spectral appearance. Absorption edges are reduced in strength, line and continuum emission features show up in different places and the gas response to continuum variation is more complicated than previously assumed. All this has immediate consequences to the analysis of the X-ray spectrum of AGNs. High- and moderate-resolution future X-ray instruments have the capability of measuring many of the predicted features. Moreover, some such features are calculated to be enough in AGN spectra to be detectable even with existing experiments, such as *ROSAT* and *BBXRT*.

I am grateful to the USA NRC for supporting my visit to the Goddard Space Flight Center through a senior research fellowship. I have benefited from numerous conversations with members of the Goddard X-ray group, in particular H. Awaki, E. Boldt, M. Corcoran, C. Done, R. Edelson, I. George, T. Kallman, G. Madejski, F. Marshall, R. Mushotzky, R. Petre, A. Rots, G. Reichert, P. Serlemitsos, J. Turner, and K. Weaver. I also thank A. Pradhan, J. Raymond, and D. Pequignot for providing useful information.

REFERENCES

Arnaud, M., & Raymond, J. C. 1992, ApJ, 398, 394
Band, D. L., Klein, R. I., Castor, J. I., & Nash, J. K. 1990, ApJ, 362, 90
Bai, T., & Ramaty, R. 1978, ApJ, 219, 705
Done, C., Mulchaey, J. S., Mushotzky, R. F., & Arnaud, K. A. 1992, ApJ, 395, 275
Ferland, G. J., & Rees, M. J. 1988, ApJ, 332, 141
George, I. M., & Fabian, A. C. 1991, MNRAS, 249, 352
Gould, R. J. 1978, ApJ, 219, 250
Halpern, J. P. 1984, ApJ, 281, 90
Holt, S. S., Mushotzky, R. F., Becker, R. M., Bolt, E. A., Szymkowiak, A. E., & White, N. E. 1980, ApJ, 241, L13
Krolik, J. H., & Kallman, T. R. 1984, ApJ, 286, 366
Kaastra, J. S., Mewe, R., & Brinkman, A. C. 1989, in Proc. 23d ESLAB Symp. on Two-Topics in X-Ray Astronomy, ed. J. Hunt & B. Battrick (Noordwijk: ESA), 951
Laor, A. 1990, MNRAS, 246, 369
Liedahl, D. A., Kahn, S. M., Osterheld, A. L., & Goldstein, W. H. 1990, ApJ, 350, L37
Lightman, A. P., & White, T. R. 1988, ApJ, 335, 57
Marshall, F. E., et al. 1993, ApJ, 405, 168
Mathews, W. G., & Ferland, G. J. 1987, ApJ, 323, 456
Matt, G., Perola, G. C., & Piro, L. 1991, A&A, 247, 25
Mewe, R. 1991, Astron. Ap. Rev., 3, 127
Netzer, H. 1990, in Active Galactic Nuclei (Berlin: Springer)
Pan, H. C., Stewart, G. C., & Pounds, K. A. 1990, MNRAS, 242, 177
Pequignot, D., Petitjean, P., & Boisson, C. 1991, A&A, 251, 680
Raymond, J. C., & Smith, B. W. 1977, ApJS, 35, 419
Rees, M. J., Netzer, H., & Ferland, G. J. 1989, ApJ, 347, 640
Reichert, G. A., Mushotzky, R. F., & Holt, S. S. 1986, ApJ, 303, 87
Reichert, G. A., Mushotzky, R. F., Petre, R., & Holt, S. S. 1985, ApJ, 296, 69
Reilman, R. F., & Manson, S. T. 1979, ApJS, 40, 815
Shull, J. M., & Van Steenberg, M. 1982, ApJS, 49, 351
Turner, T. J., Weaver, K. A., Mushotzky, R. F., Holt, S. S., & Madejski, G. M. 1991, ApJ, 381, 85
Wachter, K. W., Strauss, M. A., & Filippenko, A. V. 1988, ApJ, 330, 91
Yaqoob, T., & Warwick, R. S. 1991, MNRAS, 248, 773
Yaqoob, T., Warwick, R. S., & Pounds, K. A. 1989, MNRAS, 236, 153